Advances in Reliability, Safety and Security, Part 9 – Kołowrocki, Dąbrowska (eds.)
 ISBN 978-83-68136-21-0 (printed), ISBN 978-83-68136-08-1 (electronic)

Advances in Reliability, Safety and Security

ESREL 2024
Monograph Book Series

Analyzing Spectrogram Parameters' Impact On Wear State Classification For Milling Tools

Neha Patel, Rajiv Nandan Rai

Indian Institute of Technology, Kharagpur, India

Abstract

Machining, a commonly employed production method, faces specific challenges like chatter and severe tool wear, which have the potential to disrupt the manufacturing process. Detecting tool wear state in machining is crucial to identify before its value reaches the threshold limit, to ensure surface quality, productivity, and prevent workpiece degradation. The detection of tool wear states in machining, identified by unbalanced vibrations during machining, shows difficulties in handling through traditional approaches due to its non-stationary and complicated nature. To tackle these challenges, this study employs time-frequency methodologies to convert signals into spectrogram images, specifically for four states related to the condition of cutting tools: initial wear, steady state wear, severe wear, and worn-out. This research suggests examining the spectrogram parameters' impact on the successful classification of tool wear states during machining, utilizing the architecture of CNN-MobileNet model. This deep learning technique allows for the automatic and precise identification of intricate fault patterns, thereby improving the effectiveness of fault detection methods. The study employs a milling dataset comprising three cutters C1, C4, & C6, and utilizes the CNN-MobileNet architecture to assess the variation of spectrogram parameters' impact on validation loss and accuracy for tools' wear state classification. The vibration signals are first transformed into spectrogram images, and then a systematic analysis is performed to assess the impact of different DFTs points, overlapping percentages, and windows sizes on fault classification accuracy. This analysis is carried out across three cutting tools. The findings suggest optimal parameter configurations for spectrograms, ensuring a fault classification accuracy within the range of 95-96%. The significant contribution of this study lies in offering a thorough examination of parameter impact on the accuracy of wear states detection, and help in preventing the cutting tools catastrophic failure. The paper's results focus on the meticulous selection of spectrogram parameters for the accurate detection of tool wear states, providing valuable insights. This study aims to support industries in improving the reliability of their machining operations, addressing issues related to economic consideration, quality assurance and safety.

Keywords: cutting tools, machining, wear states, fault classification, spectrogram

1. Introduction and literature survey

Machining is a crucial process in the field of manufacturing industries, executed through the precise cutting tools. During machining, the cutting tools experience extreme wear and degradation due to mechanical, thermal, and chemical stresses. As a result, the poor quality of the machined surface and higher tolerance errors are observed during machining processes that are milling, drilling, and turning (Yang and Li, 2018; Zhang et al., 2022). This study mainly focuses on milling which is an intermittent machining process, utilizing a multi-flute cutter that induces temperature variations and vibration at the cutting edge (Li et al., 2023). The vibration generates a dynamic wave at the tool edge, resulting in poor surface finish. The wear of the cutting tools might cause excessive vibration during machining, which can impact the material removal rate and perhaps lead to tool's tip failure (Bai et al., 2023). Hence, to mitigate the adverse effects of tool damage on the machining process, detection of cutting tools' wear state through online monitoring systems is essential. An effective condition monitoring system can reduce downtime by 10–40% and enhance workpiece quality (Peng et al., 2020).

An accurate assessment of the tool wear state can be performed in real-time by examining several signals such as cutting force, vibration, acoustic emission, and spindle motor current. The signals are further used to extract features in the time, frequency, and time-frequency domains (Entezami 2021). Subsequently, these

features encompass various decision-making algorithms to assess the status of the cutting tools. Patange et al., (2021) proposed a machine learning method to determine the state of a milling cutter by using selected significant features from a decision tree and classified using a random forest tree technique for various tool conditions. The vibration signal is used to extract statistical features, and then dimensionality reduction is performed using the J48 classifier (Bajaj et al., 2021; Khade et al., 2021). Kothuru et al. (2018) employed acoustic signals in the frequency domain to develop a multiclass support-vector machine (SVM) for detecting tool wear in end milling. In a similar manner, Hu et al. (2019) classified tool wear into four distinct states by considering mechanisms, wear rate, and tool life and utilized a v-SVM model to achieve efficient monitoring of tool wear. It is evident that vibration signals in tool wear often exhibit dynamic behaviour and non-stationarity, making them challenging to handle using traditional time and frequency domain-based statistical features. Hence, to handle this challenge Karabacak (2023) employed spectrograms for classifying tool wear states, leveraging their utility in extracting relevant features from signals generated during machining. Experimental results have shown that spectrogram image-based methods provide high diagnostic accuracy for bearing fault signals in complex conditions of variable rotational speeds (Pham et al., 2020) and under low Signal-to-Noise Ratio (SNR) levels (Jiang et al., 2021). Specifically, features derived from spectrogram images play a crucial role in assessing machining stability, as they effectively capture the rise in energy allied to tool wear (Kale et al., 2023).

A significant gap identified in the existing literature while using spectrogram images is their consistent time-frequency resolution across all types of signals. The lack of variation in this context presents challenges in accurately resolving ultra-band and wide-band signals, perhaps resulting in inadequate spectrogram resolution (Lukin and Todd 2006). Because of this, the selection of an optimal windows size, overlap percentage, and discrete Fourier transform (DFT) points are very important in the spectrogram image-based fault diagnosis (Muller et al., 2011). The window size determines the balance between time resolution and frequency resolution in the spectrogram, where, larger window size provides better frequency resolution but lesser time resolution, and vice versa (Leiber et al., 2022). The size of the window can also impact the effectiveness with which specific signal characteristics are captured. For example, a greater window size could be more effective in capturing lower frequency elements, whereas a smaller window size might be more suitable for capturing higher frequency components. When applying spectrograms to short signals, achieving a balance between the window size and the degree of pixelation along with the time axis is crucial. This balance can be attained by incorporating overlapping parameters (Zhang 2019). Enhancing the overlap by 50% or 90% increases the visual clarity of information, but does not boost the resolution, which is determined by the quantity of DFT points. The number of DFT points determines the frequency resolution of the spectrogram (Malarvannan et al., 2023). Hence, examining the correlation among window size, overlapping, and number of DFT points is essential for maximizing accuracy of wear states classification and establishing selection of parameters, which is found limited in the reviewed literature. In addition, spectrogram images are commonly classified using convolutional neural networks (CNNs) because of their capacity to efficiently acquire spatial hierarchies of characteristics (Kumari et al., 2021). Therefore, this research employs the MobileNet architecture (Peng 2023) because of its advantage of being lightly loaded with parameters and rarely utilized in the classification of wear states in cutting tools.

The main contribution of the paper is to scrutinize the main effect and interaction effect of windows size, overlap percentage, and number of DFT points on validation loss and accuracy of wear state classification. This specific aspect has been inadequately addressed in the current literature concerning the classification of cutting tool wear states. This research paper additionally contributes to the field of CNN-MobileNet architecture based comprehensive image classification, and it demonstrates an analysis to evaluate spectrogram parameters' impact on the accuracy and validation loss of tool wear states classification model. This paper further investigates the outcomes through the utilization of main and interaction effect plots. Then, these plots are used to provide recommendations for optimal parameter settings and also explore the influence of parameter variations on validation loss and mean accuracy.

Therefore, this paper proposes a comprehensive approach for indicating the appropriate spectrogram image parameters that are selectively improved to capture the tool wear state during machining with utmost accuracy. The analysis of tool wear severity in machining tools using spectrogram parameters are likely to benefit the scientific community and industries to prevent tool breakage and extension of tool lifespan. This will certainly decrease the cycle time of machining processes, resulting in improved productivity and throughput.

The forthcoming sections are organized in the following manner: Section 2 outlines the proposed methodology, Section 3 provide results and corresponding discussion, while Section 4 offers the conclusion for the paper.

2. Methodology

The proposed methodology begins with the acquisition of the milling dataset on tool wear, which is subjected to preprocessing and categorized into four distinct labels, as illustrated at Figure 1. Subsequently, spectrogram images are derived from the dataset, employing diverse parameters such as windows size, overlap percentage, and number of DFT points. The dataset is then partitioned into training and testing sets, serving as inputs for the CNN-MobileNet architecture (Peng 2023) model designed for classification purposes. Finally, a comprehensive accuracy and validation loss analysis is conducted to assess the performance of the model across various configurations of spectrogram parameters.

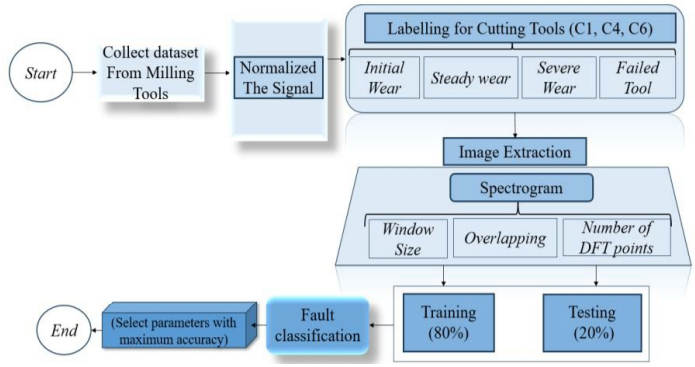

Fig. 1. Proposed methodology.

2.1. Dataset description

The proposed methodology in this paper is verified by utilizing the 2010 PHM Data Challenge dataset (Xinghui Li 2021; Li et al., 2009), which originated from experiments conducted under consistent operating conditions. The experimental configuration, as depicted in Figure 2, utilized a three-flute ball nose tungsten carbide milling cutter, with operational parameters detailed in Table 1. Cutting forces along the x, y, and z axes are gauged through a three-component platform dynamometer strategically positioned between the workpiece and the machining table. Concurrently, machine tool vibrations during cutting are monitored utilizing three accelerometers affixed to the workpiece, capturing vibrations in the x, y, and z directions. Simultaneously, an acoustic emission sensor captures the sound emanating from the cutting process. The acquired vibration, force, and acoustic emission signals undergo preprocessing via a charge amplifier and data acquisition system before being transmitted to the PC. The data acquisition system functions at a sampling rate of 50 kHz. Following each surface machining operation, the flank wear of each flute is measured, with seven channels capturing signals, and the flank wear is designated as the target value.

Table 1. Experimental parameters

Spindle speed	Feed Rate	Radial Depth of Cut	Axial Depth of cut	Sampling Frequency
10,400 rpm	1555 mm/min	0.125 mm	0.2 mm	50KHz

In this investigation, we are focusing on the vibration signal for further analysis, as it is a widely recognized indicator used by many researchers for tool wear state classification. The directory of this dataset encompasses around 315 distinct data-log files, each corresponding to an individual cutting operation. Each operation includes a 'wear' file documenting the wear measurement after each cut, rounded to the nearest 10^{-3} mm for six cutters, namely C1, C2, C3, C4, C5, and C6. In datasets C1, C4, and C6, wear measurements for the three flutes are concurrently recorded, while other datasets lack this information. Consequently, records from C1, C4, and C6 are suitable for classifying the tool wear states. Further to this, data are segregated and divided into 80% for training and 20% for testing.

Additionally, the signals undergo preprocessing and are classified into four distinct labels. These labels are defined according to the wear rate profile (Hu et al., 2019). In this paper, tool wear is categorized into four states, as depicted in Figure 3 for cutter C1. State 1 encompasses 1^{st} to 25^{th} cut, characterized by initial wear rate at the start of the operation. State 2 spans 25^{th} to 154^{th} cut, indicating steady wear and showing very low rate of wear.

State 3 occurs from 154th to 298th cut, marked by rapid tool wear with a rate exceeding 0.002 mm/cut number, reaching 0.0045 mm/cut number before tool failure. Finally, State 4 is defined from the 298th to the 315th cut, where tool wear surpasses the tool life criterion i.e., 165mm, signifying tool wear-out. Similarly, for the other cutters C4 and C6, the states are illustrated in Table 2 along with their respective tool wear values.

After categorizing tool wear states, spectrogram images are produced by utilizing vibration signals. The subsequent section provides an explanation of the Short-Time Fourier Transform (STFT) spectrogram utilized to produce spectrogram images.

Fig. 2. Experimental setup (Li et al., 2009).

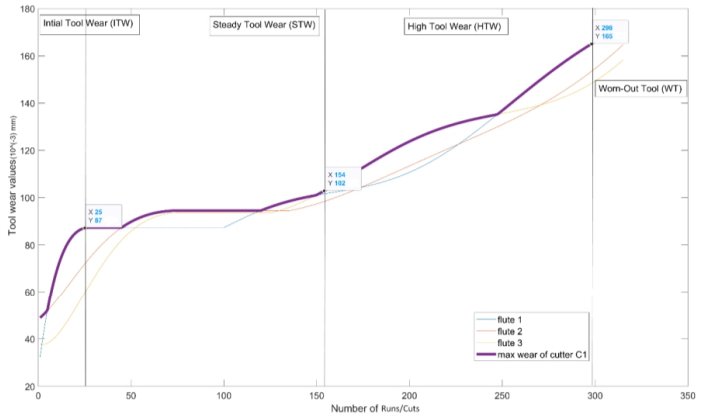

Fig. 3. Represents tool wear states.

Table 2. Cutting tools wear states limits.

Wear States	ITW (10^{-3} mm)	STW (10^{-3} mm)	HTW (10^{-3} mm)	WT (10^{-3} mm)
Cutter C1	<87	87-102	102-165	>165
Cutter C4	<65	65-104	104-165	>165
Cutter C6	<106	106-131	131-165	>165

2.2. Short Term Fourier Transform Spectrogram (STFT)

The Short-Term Fourier Transform (Kehtarnavaz, 2011) is a technique employed for signal analysis in both the time and frequency domains. The process entails dividing a signal in the time domain into smaller sections,

usually with the use of a windows function, and subsequently calculating each segment Fourier transform to expose its frequency characteristics. The window position is systematically adjusted throughout the complete dataset to compute Short-Time Fourier Transform coefficients at different locations of time-frequency plot. These standardized squared magnitudes of coefficients are commonly visualized as a spectrogram. The spectrogram serves as a visual representation illustrating the distribution of the energy of the signal across various frequencies with time. The STFT can be mathematically expressed as follows in (1).

$$S(t,f) = \int_{-\infty}^{\infty} s(\tau)w(\tau - t)e^{-j2\pi f\tau}d\tau \quad (1)$$

The expression $S(t, f)$ denotes the coefficients of STFT at a certain frequency f and time t. The input time-domain signal is represented by $s(\tau)$, while $w(\tau\text{-}t)$ represents a windowing function. The imaginary unit is denoted by j, and the integration is conducted over all time values denoted by τ.

This study investigates the influence of spectrogram characteristics, including windows size, overlap percentage, and number of DFT points, on the precision of a wear states classification model. Table 3 represents the parameters' levels are considered for this paper.

Table 3. Spectrogram parameters levels.

Spectrogram parameters\levels	Level 1	Level 2	Level 3	Level 4
Windows size	28	64	100	200
Overlap percentage	-	25%	50%	75%
Number of DFT points	128	256	512	1024

Table 4. CNN-MobileNet architecture.

Type	Stride value	Filter shape	Input size
Standard convolution	2	3×3×3×32	224×224×3
Depthwise separable convolution	1	3×3×32	112×112×32
Standard convolution	1	1×1×32×64	112×112×32
Depthwise separable convolution	2	3×3×64	112×112×64
Standard convolution	1	1×1×64×128	56×56×64
Depthwise separable convolution	1	3×3×128	56×56×128
Standard convolution	1	1×1×128×128	56×56×128
Depthwise separable convolution	2	3×3×128	56×56×128
Standard convolution	1	1×1×128×256	28×28×128
Depthwise separable convolution	1	3×3×256	28×28×256
Standard convolution	1	1×1×256×256	28×28×256
Depthwise separable convolution	2	3×3×256	28×28×256
Standard convolution	1	1×1×256×512	14×14×256
		3×3×512	
5 × Depthwise separable convolution	1	1×1×512×512	14×14×512
Convolution			14×14×512
Depthwise separable convolution	2	3×3×512	14×14×512
Standard convolution	1	1×1×512×1024	7×7×512
Depthwise separable convolution	2	3×3×1024	7×7×1024
Standard convolution	1	1×1×1024×1024	7×7×1024
Average pool	1	Pool 7×7	7×7×1024
Fully connected	1	1024×1000	1×1×1024
Softmax activation function	1	Classifier	1×1×1000

2.3. CNN-MobileNet architecture

MobileNet is a convolutional neural network (CNN) architecture (Peng 2023) specifically developed to create neural network models that are efficient and lightweight as shown in Table 4. It is particularly suitable for mobile and edge devices that have low processing resources. MobileNet, developed by Google researchers in 2017, employs depthwise separable convolutions to decrease the number of parameters and calculations. This results in faster inference and a smaller memory requirement compared to conventional CNN architectures. Initially, features are extracted through convolution and pooling layers, generating feature maps that capture the image's distinctive characteristics. Notably, MobileNet utilizes depthwise separable convolutions, dividing standard convolutions into depthwise and pointwise convolutions. Depthwise convolutions apply filters

independently to each input channel, while pointwise convolutions merge results through 1x1 convolutions, significantly reducing computational costs while maintaining model accuracy. The feature maps from the last convolution layer are then flattened into one-dimensional vectors to facilitate input into fully connected layers. The final classification occurs at the output layer, employing a softmax activation function to produce a probability distribution over classes, with the highest probability determining the output prediction.

3. Results and discussion

The proposed methodology in this paper enables milling datasets to generate spectrogram-based images with varying levels of parameters, as outlined in Table 3. Subsequently, the impact of varying windows size on the spectrogram images for cutter C1 is depicted in Figure 4, while keeping overlap percentage and number of DFT points constant. Similarly, the effects of overlap percentage and number of DFT points on spectrogram images are also examined that provide insights into how spectrogram parameters influence image representation. These based spectrogram images are then fed into a CNN-MobileNet architecture (Section 2.3) to assess the impact of these varying parameters on the validation loss and accuracy of tool wear state classification for each cutting tool. In this paper, cross-entropy which is commonly used loss function in machine learning for classification is considered as a validation loss function. It is employed to measure the dissimilarity between the predicted probability distribution and the actual distribution (Zhou et al., 2019). The subsequent paragraphs explore into the observed discrepancies in accuracies and validation loss for these parameters.

After evaluating the validation loss and accuracy of tool wear states classification, a thorough analysis is performed by main effect and interaction effect plots. Figures 5, 6, and 7 represent the main effect plots, which are used to evaluate the association between the response variable i.e., validation loss or accuracy, and predictor variables i.e., windows size, overlap percentage, and number of DFT points. The information depicted in the plots correspond to the response variable means for each discrete combination of factor levels. More precisely, Figures 5(a), 6(a), and 7(a) represent the main effect plots of classification accuracies for cutting tools' wear states achieved by varying spectrogram parameters with cutter C1, C4, and C6, respectively. The main effect plots of validation losses derived from varying spectrogram parameters with cutters C1, C4, and C6 are represented by Figures 5(b), 6(b), and 7(b), respectively. When examining cutter C1 in Figures. 5(a) and 5(b), the most accurate results and lowest validation losses are obtained at a window size of 200, with 75% overlap, and employing 1024 DFT points. These settings outperform other factor levels. Similarly, cutters C4 and C6 also exhibit the same main effects as cutter C1 for accuracy and validation loss as shown in Figures 6 and 7.

The statistics from these figures advise that increasing the windows size, overlap percentage, and number of DFT points result in improving accuracy and reducing validation loss for detection of tool wear states. The impact of DFT points on fault classification accuracy and validation loss has been found to be nearly negligible. Therefore, the influence of different DFT points on the fluctuation of accuracy and validation loss is almost insignificant, as evidenced by the practically horizontal lines. It is advisable to validate the conclusions drawn from main effect plots by examining interaction plots before making any definitive assessments. Relying solely on main effect plots for conclusions may not always be reasonable. The following paragraph will present the interaction plots for a more thorough examination.

The interaction plot in Figure 8(a) demonstrate that cutter C1 achieves the maximum mean accuracies at certain combinations: a window size of 100 with a 75% overlap, and DFT points at 512 or 1024. Similarly, in Figure 8(b), the interaction plots for mean validation loss show that the minimum validation loss occurs at the combination of window size 200, overlap percentage 75%, and number of DFT point 1024 for cutter C1, which compliment main effect plots. Similarly, In Figures 9(a) and 10(a), the maximum accuracy is observed at 100 or 200 window sizes, 75% or 50% overlapping percentages, and 1024 DFT points for cutter C4 and C6. Conversely, Figures 9(b) and 10(b) demonstrate the minimum validation loss at a window size of 200, overlapping percentages of 50% or 75%, and 1024 DFT points for cutter C4 and C6.

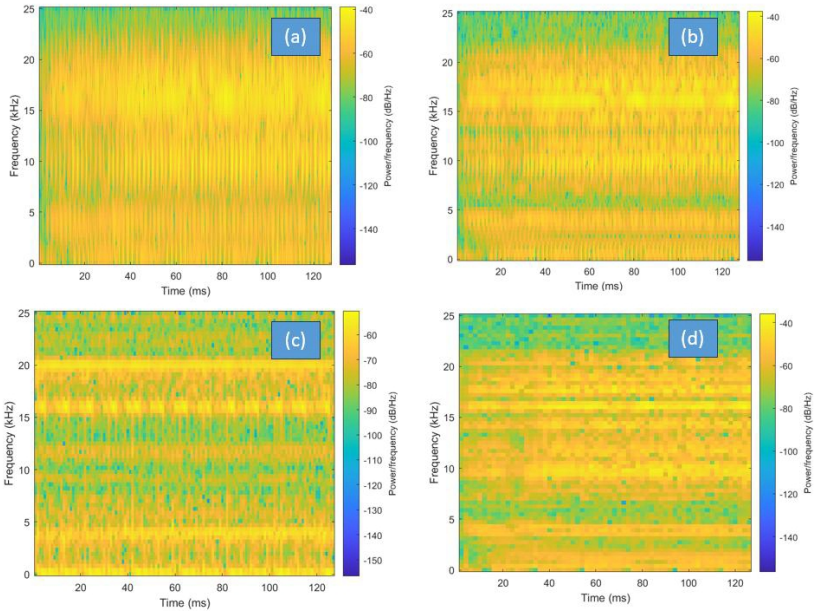

Fig. 4. Represent effect of windows sizes on spectrogram images where 25% overlapping, 215 DFT points and windows sizes are (a) 28, (b) 64, (c) 100, and (d) 200.

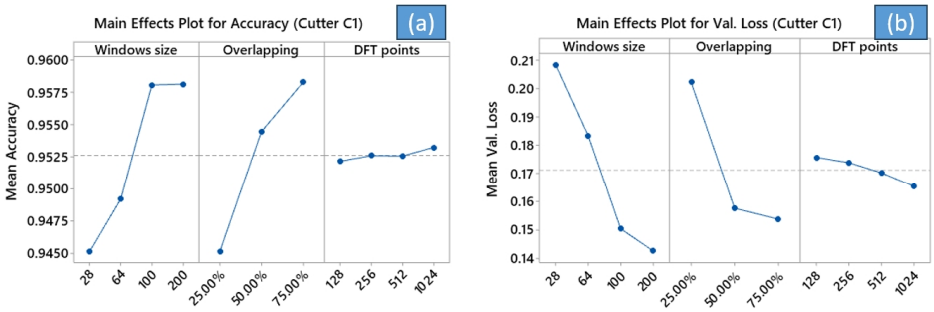

Fig. 5. Represent main effect plots of cutter C1 where responses are (a) mean accuracy and (b) validation loss.

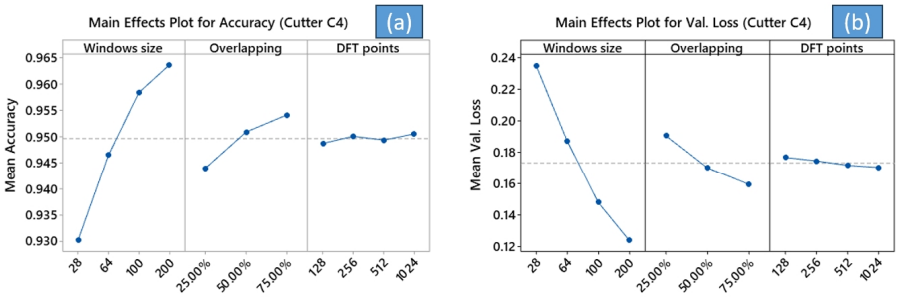

Fig. 6. Represent main effect plots of cutter C4 where responses are (a) mean accuracy and (b) validation loss.

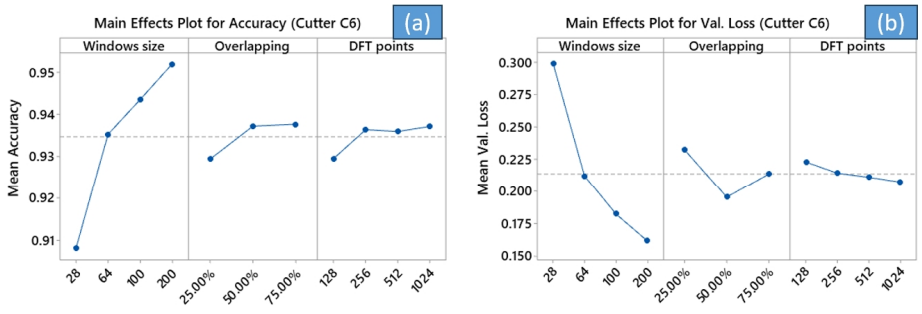

Fig. 7. Represent main effect plots of cutter C6 where responses are (a) mean accuracy and (b) validation loss.

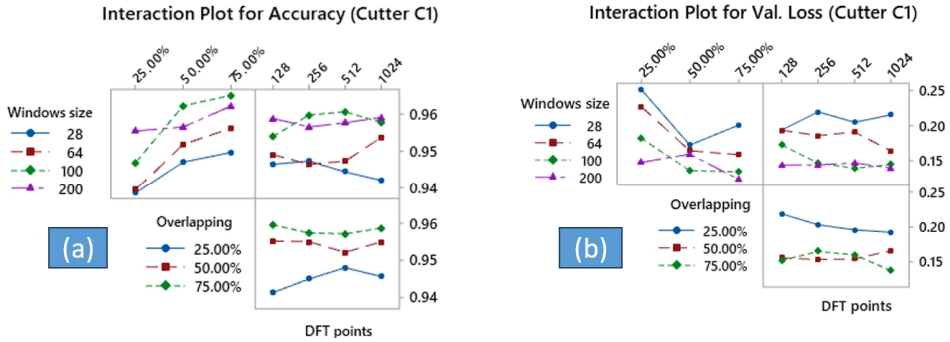

Fig. 8. Represent interaction effect plots of cutter C1 where responses are (a) mean accuracy and (b) validation loss.

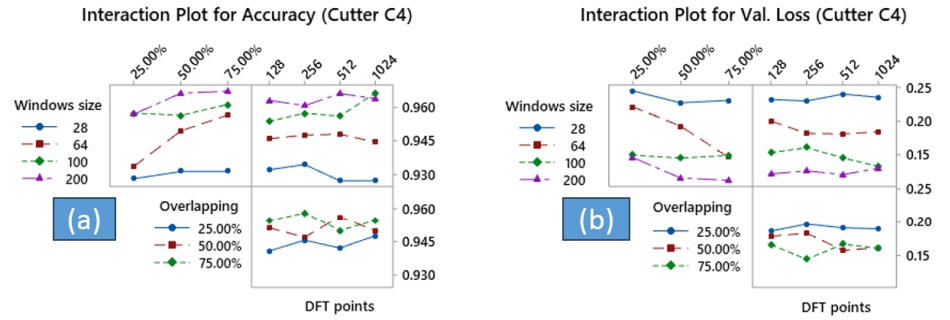

Fig. 9. Represent interaction effect plots of cutter C4 where responses are (a) mean accuracy and (b) validation loss.

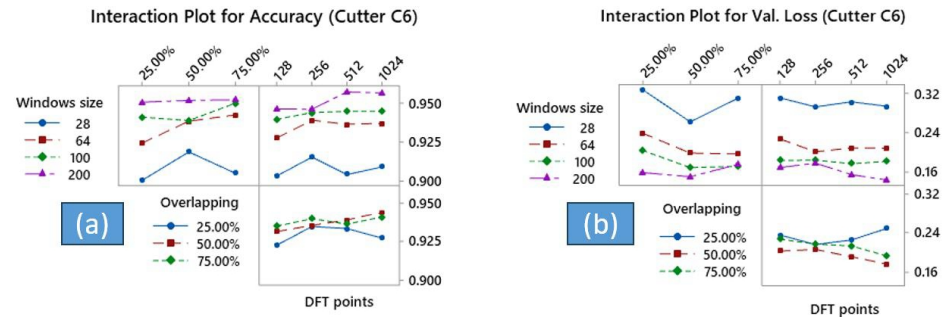

Fig. 10. Represent interaction effect plots of cutter C6 where responses are (a) mean accuracy and (b) validation loss

The interaction plot results complement those of the main effect plots, highlighting the pronounced impact of window size, while the influence of overlapping and DFT points is comparatively less. DFT points exhibit less variability in validation loss and accuracy, evident from the horizontal line pattern. The maximum accuracy achieved is 96.79% for cutter C1, 97.01% for cutter C4, and 96% for cutter C6, corresponding to their optimal spectrogram parameters. The respective confusion matrices are presented in Figure 11.

Based on the above corresponding observations, the main effect plots and interaction plots indicate that accuracy and validation loss are influenced differently by window size, overlapping percentage, and DFT points. These findings offer valuable insights for optimizing the fault classification process under different conditions.

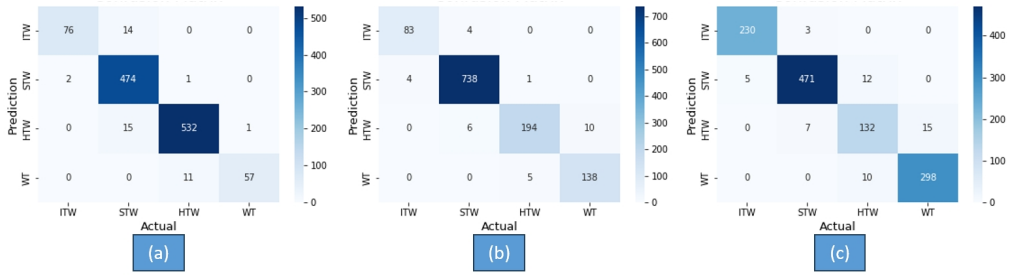

Fig. 11. Confusion matrix for tool wear state classification with (a) cutter C1, (b) cutter C4, and (c) cutter C6.

4. Conclusion

This study investigates the influence of variation of the spectrogram parameters on the wear states classification accuracy and validation loss in machining operations, using three different cutters: C1, C4, and C6 with same operating conditions. The data collected from milling is transformed into spectrogram images by using various windows size, overlap percentages, and number of DFT points. Then, CNN-MobileNet model is employed for the classification of tool wear states. Subsequently, accuracies and validation losses are analyzed through interaction and main effect plots. These plots provide a clear understanding of how the parameters impact accuracies and losses, providing significant insights for parameter selection.

The main findings of this analysis on tool wear states classification using variations in spectrogram parameters can be summarized as follows:

- the accuracy and validation loss are influenced by the overlapping percentage, windows size, and DFT points;
- the results demonstrated a positive correlation between the increase in overlapping percentage, windows size, and DFT points, and the corresponding increase in accuracy;
- the results demonstrated that augmenting the windows size, incorporating overlapping percentage, and increasing the number of DFT points led to a reduction in validation loss;
- the impact of altering the number of DFT points on the variability of accuracy and validation loss is nearly negligible;
- the utilization of a window size of 100 or 200 in conjunction with 1024 DFT points yielded superior accuracies, ranging from 95 to 97%;
- the analysis showed that using 75% overlapping with 1024 DFTs consistently produced less validation losses as compared to alternative overlap percentage options.

The identified optimal parameter configurations can be employed to effectively identify severe wear states through spectrogram images and, simultaneously, minimize validation losses. This has the potential to prevent tool breakage by accurately detecting and mitigating heat generation, chatter, uneven forces, induced vibrations, and damage to the workpiece surface. This study aims to improve the machining process reliability in industries, addressing concerns related to quality, economic factors and safety. Precise cutting tool's wear state detection can contribute to enhance the line throughput and reducing process cycle time.

The future prospects of this research entail enhancing parameters setting for fault diagnosis in milling operations, investigating more deep learning approaches, and incorporating real-time monitoring systems into machining industry settings.

References

Bai, W., Y. Gao, R. Sun. 2023. Tool Wear in Vibration Assisted Machining. Pages 155–174 in W. Bai, Y. Gao, and R. Sun, editors. Vibration Assisted Machining: Fundamentals, Modelling and Applications. Springer Nature Singapore, Singapore.

Bajaj, N. S., A. D. Patange, R. Jegadeeshwaran, K. A. Kulkarni, R. S. Ghatpande, A. M. Kapadnis. 2021. A Bayesian Optimized Discriminant Analysis Model for Condition Monitoring of Face Milling Cutter Using Vibration Datasets. Journal of Nondestructive Evaluation, Diagnostics and Prognostics of Engineering Systems 5.

Entezami, A. 2021. Feature Extraction in Time-Frequency Domain for Non-Stationary Data. Pages 47–57 in A. Entezami, editor. Structural Health Monitoring by Time Series Analysis and Statistical Distance Measures. Springer International Publishing, Cham.

Hu, M., W. Ming, Q. An, M. Chen. 2019. Tool wear monitoring in milling of titanium alloy Ti–6Al–4 V under MQL conditions based on a new tool wear categorization method. The International Journal of Advanced Manufacturing Technology 104, 4117–4128.

Jiang, Q., F. Chang, C. Liu. 2021. A Spectrogram Based Local Fluctuation Feature for Fault Diagnosis with Application to Rotating Machines. Journal of Electrical Engineering & Technology 16, 2167–2181.

Kale, A. P., R. M. Wahul, A. D. Patange, R. Soman, W. Ostachowicz. 2023. Development of Deep Belief Network for Tool Faults Recognition. Sensors 23.

Karabacak, Y. 2023. Deep learning-based CNC milling tool wear stage estimation with multi-signal analysis. Eksploatacja i Niezawodnosc - Maintenance and Reliability 25.

Kehtarnavaz, N. 2011. Digital signal processing system design: LabVIEW-based hybrid programming. Elsevier.

Khade, H. S., A. D. Patange, S. S. Pardeshi, R. Jegadeeshwaran. 2021. Design of bagged tree ensemble for carbide coated inserts fault diagnosis. Materials Today: Proceedings 46, 1283–1289.

Kothuru, A., S. P. Nooka, R. Liu. 2018. Application of audible sound signals for tool wear monitoring using machine learning techniques in end milling. The International Journal of Advanced Manufacturing Technology 95, 3797–3808.

Kumari, N., S. Anwar, V. Bhattacharjee. 2021. Convolutional Neural Network-Based Visually Evoked EEG Classification Model on MindBigData. Pages 233–241 in I. Pan, A. Mukherjee, and V. Piuri, editors. Proceedings of Research and Applications in Artificial Intelligence. Springer Singapore, Singapore.

Leiber, M., A. Barrau, Y. Marnissi, D. Abboud. 2022. A differentiable short-time Fourier transform with respect to the window length. Pages 1392–1396 2022 30th European Signal Processing Conference (EUSIPCO).

Li, C., B. Li, H. Wang, D. Shi, F. Gu, A. D. Ball. 2023. Tool Wear Monitoring in CNC Milling Process Based on Vibration Signals from an On-Rotor Sensing Method. Pages 268–281 in H. Zhang, Y. Ji, T. Liu, X. Sun, and A. D. Ball, editors. Proceedings of TEPEN 2022. Springer Nature Switzerland, Cham.

Li, X., B. S. Lim, J. H. Zhou, S. Huang, S. J. Phua, K. C. Shaw, M. J. Er. 2009. Fuzzy Neural Network Modelling for Tool Wear Estimation in Dry Milling Operation. Page Conference of the Prognostics and Health Management Society.

Lukin, A., and J. G. Todd. 2006. Adaptive Time-Frequency Resolution for Analysis and Processing of Audio. Journal of The Audio Engineering Society.

Malarvannan, M., K. V. Kumar, Y. P. Reddy, P. Nikhil, D. Aishwarya, V. Ravichandiran, P. Ramalingam. 2023. Assessment of computational approaches in the prediction of spectrogram and chromatogram behaviours of analytes in pharmaceutical analysis: assessment review. Future Journal of Pharmaceutical Sciences 9, 86.

Muller, M., D. P. W. Ellis, A. Klapuri, G. Richard. 2011. Signal Processing for Music Analysis. IEEE Journal of Selected Topics in Signal Processing 5, 1088–1110.

Patange, A., J. R. 2021. Review on tool condition classification in milling: A machine learning approach. Materials Today: Proceedings.

Peng, L. 2023. Piano Players' Intonation and Training Using Deep Learning and MobileNet Architecture. Mobile Networks and Applications.

Peng, R., H. Pang, H. Jiang, Y. Hu. 2020. Study of Tool Wear Monitoring Using Machine Vision. Automatic Control and Computer Sciences 54, 259–270.

Pham, M. T., J.-M. Kim, C. H. Kim. 2020. Deep Learning-Based Bearing Fault Diagnosis Method for Embedded Systems. Sensors 20.

Xinghui Li. 2021. 2010 PHM Society Conference Data Challenge. IEEE Dataport.

Yang, S., W. Li. 2018. Surface Quality and Finishing Technology. Pages 1–64 in S. Yang and W. Li, editors. Surface Finishing Theory and New Technology. Springer Berlin Heidelberg, Berlin, Heidelberg.

Zhang, R., A. Li, X. Song. 2022. Surface quality adjustment and controlling mechanism of machined surface layer in two-step milling of titanium alloy. The International Journal of Advanced Manufacturing Technology 119, 2691–2707.

Zhang, Z. 2019. Spectral and Time-Frequency Analysis. Pages 89–116 in L. Hu and Z. Zhang, editors. EEG Signal Processing and Feature Extraction. Springer Singapore, Singapore.

Zhou, Y., X. Wang, M. Zhang, J. Zhu, R. Zheng, Q. Wu. 2019. MPCE: A Maximum Probability Based Cross Entropy Loss Function for Neural Network Classification. IEEE Access 7, 146331–146341.